Journal of Molecular Liquids 196 (2014) 26–31

Contents lists available at ScienceDirect

Journal of Molecular Liquids

journal homepage: www.elsevier.com/locate/molliq

Vibrational analysis of neat liquid *tert*-butylmethylether

K.B. Beć *, A. Kwiatek, J.P. Hawranek

Faculty of Chemistry, University of Wrocław, F. Joliot-Curie 14, 50-383 Wrocław, Poland

ARTICLE INFO

Article history:
Received 16 January 2014
Accepted 26 February 2014
Available online 14 March 2014

Keywords:
IR dispersion
Complex refractive index
Neat liquid *tert*-butylmethylether (TBME)
Thin film IR spectra
Low temperature matrix IR spectra
Anharmonic vibrational analysis
B2PLYP/N07D

ABSTRACT

Among aliphatic ethers, the most known is *tert*-butylmethylether (TBME), mainly for its significance in the fuel industry. It was the subject of numerous investigations, including industrial, environmental and medical studies. The literature however is lacking of any insightful infrared studies of TBME in neat liquid phase. In this work we determined the optical constants of TBME, from transmission studies in the IR range (11,700–560 cm^{-1}). The use of quantitative thin film recording techniques was essential due to the high absorption of neat liquids in the MIR range. Low temperature matrix investigation was also carried out, to elucidate details of the vibrational spectrum of TBME. The experiment was supported by an anharmonic vibrational analysis including the simulation of experimental spectrum, based on the B2PLYP/N07D level of theory. The chosen method delivered good results with a relatively modest computational cost.

1. Introduction

The wide utilization of *tert*-butylmethylether (TBME) in the fuel industry [1,2] in the past years led to numerous studies of its physicochemical properties [3,4], as well as environmental [5–7] and medical [8] research. In past decades the worldwide annual production volume of TBME reached 18 million tons [9], and over 3 million tons in the EU only [10]. Surprisingly the infrared properties of liquid *tert*-butylmethylether were never deeply investigated. In this work we aimed to obtain an insight into the vibrational properties of the studied ether through a broad spectral range complex refractive index measurements and a detailed vibrational analysis, with the hope to a better understanding of factors determining the vibrational spectra of TBME in the neat liquid phase. The determination of these data required the use of thin-film quantitative techniques in the MIR region due to strong absorption in the studied region. The determined $k(\nu)$ spectrum revealed broadened bands in several spectral regions. With the hope to elucidate more details in the vibrational spectrum of TBME, a low temperature matrix isolation investigation was carried out. Experimental data were supported by a detailed anharmonic vibrational analysis. The final band assignment procedure was based on a spectrum modeled with the use of the DFT-B2PLYP/N07D computational method and also PED analysis. The obtained results allowed for a detailed band identification in the vibrational spectrum of *tert*-butylmethylether.

The results of investigation reported here are also indispensable for the determination of high frequency dielectric properties of *tert*-butylmethylether in the liquid phase.

2. Experimental

The TBME sample was of the highest purity available from Aldrich, additionally dried and stored over molecular sieves under nitrogen. The density of TBME measured on an Anton Paar DMA 48 density meter was 0.7353 $g \cdot cm^{-3}$ at 298.15 K and the refractive index at sodium D-line was 1.36684 also at 298.15 K.

NIR and MIR spectra were recorded on a Nicolet Magna 860 FT-IR/Raman spectrometer. To minimize the effect of possible drift, the empty chamber was measured as a reference spectrum before and after the sample measurement. All measurements were carried out at controlled temperature 298 K.

Due to strong absorption bands, the MIR spectra were recorded in thin film cells assembled for the purpose of this work from KBr windows polished to high flatness, monitored in sodium light on a glass optical flat. The spacers were prepared out of aluminum foils of required thickness. The geometrical parameters of the cell cavity were determined by fitting the experimental interference spectrum of the empty cell with the theoretical ones, using the procedure based on the earlier derived algorithm. Several KBr cells were used with a thickness ranging from 4 to 8 μm. The resolution was set at 0.5 cm^{-1} and a scan number of 512 was chosen to ensure a good signal to noise ratio.

Spectra in the NIR range were measured on the same instrument. A CaF_2 beamsplitter with the MCT-A detector (in the region 11,700–8000 cm^{-1}) and DTGS detector (in the 8000–4000 cm^{-1} region). The resolution was maintained on a 0.5–1 cm^{-1} level, depending on the recorded subregion. Thermostated quartz cells (Hellma) of 5 and 10 mm thickness were used in the upper NIR region (11,700–8000 cm^{-1}); in the lower region, cells of 0.1 and 0.5 mm thickness were used. The absorbance spectrum of the liquid was obtained by subtraction of the empty

* Corresponding author. Tel.: +48 71 3757 249; fax: +48 71 3282 348.
E-mail address: krzysztof.bec@chem.uni.wroc.pl (K.B. Beć).

http://dx.doi.org/10.1016/j.molliq.2014.02.028
0167-7322/

cell spectrum from the spectrum of the cell filled with the liquid. Subsequently, the absorbance spectrum was recalculated to yield the spectrum of the absorption index $k(\nu)$.

FT-Raman spectra were measured on a Nicolet Magna 860 FTIR spectrometer interfaced with a FT-Raman accessory. The samples were illuminated by a Nd:YVO_4 laser line at 1.064 nm with a power of 0.2–0.3 W. A CaF_2 beamsplitter was used in combination with an InGaAs detector. The interferograms were averaged over 1024 scans. The resolution of the spectra was 2 cm^{-1}.

Infrared spectra of TBME in argon and nitrogen matrixes were recorded in a reflection mode on a Bruker 113v FT-IR spectrometer equipped with a liquid N_2 cooled MCT detector (4000–400 cm^{-1}). The resolution of collected spectra was set as 0.5 cm^{-1} and the concentration of TBME/matrix gas mixtures varied in the range 1/100–1/800. Gas mixtures were prepared by standard manometric techniques and sprayed onto a gold-plated copper mirror held at 17 K during matrix deposition by a closed cycle helium refrigerator (Air Products, Displex 202A). The matrixes were maintained at the temperature of 12 K during infrared spectra collection. The spectra of matrixes after their annealing to 33 K for 10 min were also recorded.

3. Data processing

From the transmission spectra in the entire measured region, the spectra of both components of the complex refractive index:

$$\hat{n}(\nu) = n(\nu) + ik(\nu) \quad (1)$$

were obtained by the use of the procedure described previously [11,12]; $i = \sqrt{-1}$ and ν denotes wavenumbers [cm^{-1}] throughout this work. The spectrum was processed as a whole from 11,700 to 560 cm^{-1}. To begin with, the experimental $k(\nu)$ spectrum was corrected for dispersion distortion. To ensure a good accuracy for the $k(\nu)$ spectrum, the reference point needed for the preliminary processing of data with the use of the dispersion distortion correction procedure was taken at the sodium D-line (589.6 nm). At the second stage, the $n(\nu)$ spectrum was calculated using several values of the refractive index in the visible region and the modified Kramers–Krönig procedure [13].

The spectra of the complex refractive index are required for the determination of high frequency dielectric properties of studied liquid, which are in progress. Moreover, the accurate determination of the absorptive properties of a liquid can be based only on the absorption index spectrum $k(\nu)$, because of strong distortion of thin layers transmission spectra [11].

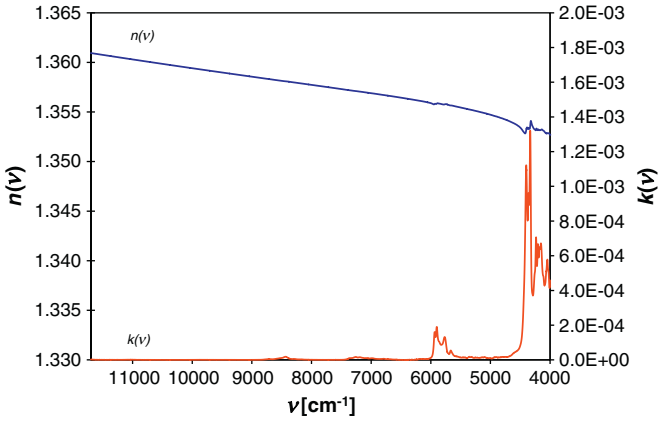

Fig. 1. Spectrum of the complex refractive index of TBME in the NIR range (11,700–4000 cm^{-1}).

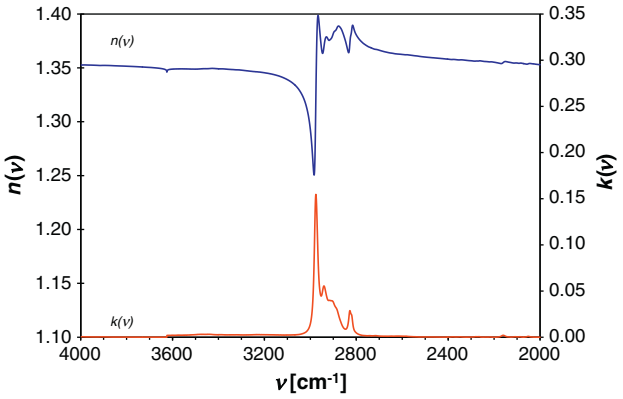

Fig. 2. Spectrum of the complex refractive index of TBME in the upper MIR range (4000–2000 cm^{-1}).

4. Results and discussion

4.1. Complex refractive index in the NIR range (11,700–4000 cm^{-1})

The complete spectrum of the complex refractive index of TBME in the measured NIR range (11,700–4000 cm^{-1}), covering the first and second overtone regions, is presented in Fig. 1.

As can be seen for the studied ether, the NIR bands are very weak except for bands in the region 6000–4000 cm^{-1}. In general, the range between 6000 and 5600 cm^{-1} reflects well the doubled 3000–2800 cm^{-1} region. The analysis of overtones for the studied molecule was not the aim of this work and will not be presented here. However, the $\hat{n}(\nu)$ spectrum had to be determined in the NIR region, since its knowledge is essential for an accurate determination of the $\hat{n}(\nu)$ spectrum in the MIR region [13].

4.2. Complex refractive index in the MIR range (4000–560 cm^{-1})

Spectra of the complex refractive index of TBME separated into the upper MIR region (4000–2000 cm^{-1}) and lower MIR region (2000–560 cm^{-1}) can be found in Figs. 2 and 3, respectively. The detailed discussion of the MIR range will be presented later in this paper. The Raman spectrum is presented in Fig. 4.

4.3. Matrix isolation studies

The determined absorption index spectrum reveals several broadened bands, mainly in the 2940–2870 cm^{-1} region and in the 1500–1350 cm^{-1} region. With the aim to achieve a higher level of detail

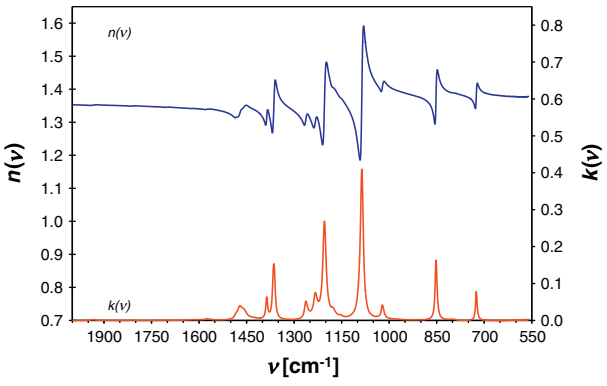

Fig. 3. Spectrum of the complex refractive index of TBME in the lower MIR range (2000–560 cm^{-1}).

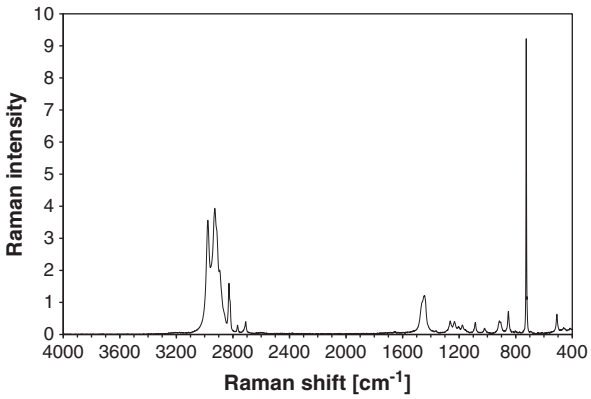

Fig. 4. Raman spectrum of liquid TBME.

in the vibrational spectrum of *tert*-butylmethylether, the IR recordings in low temperature gas matrixes were performed. The obtained exemplary spectra recorded in the Ar matrix (of concentrations 1/100 and 1/400) at 12 K are presented in Fig. 5. The spectra in the N_2 matrix were recorded as well, however they did not differ in general and therefore will not be reported here. Let's also note that the spectra remained similar before and after annealing. In Figs. 6 and 7 we present the details of both the $k(\nu)$ and the low temperature matrix spectrum in spectral ranges containing the aforementioned bands that were investigated in particular. The detailed discussion of the results will be presented in Section 4.5.

Moreover, the results of matrix isolation studies indicate that the concentration of TBME plays generally no role in the forming of its vibrational spectrum. A similar conclusion can be drawn from comparing the $k(\nu)$ spectrum with the absorption spectrum of TBME solution in carbon tetrachloride (Fig. 8). The similarity of spectra determined in this work suggest that the observed effect is in fact the property of the molecule itself rather than any conceivable concentration effect. A relatively feeble temperature dependence of IR spectra of aliphatic ethers was also reported earlier in the literature [14].

4.4. Anharmonic vibrational analysis and modelling of IR spectrum

To achieve an accurate simulation of experimental spectra the use of anharmonic calculations on relatively high level is inevitable. In our previous studies [15] we found the hybrid DFT functional B2PLYP with the N07D basis set as exceptionally valuable, considering the accuracy of calculated frequencies and computational cost. Our findings confirm the reported in the literature advantages of this discussed computational method [16]. The detailed band assignments in the vibrational spectrum

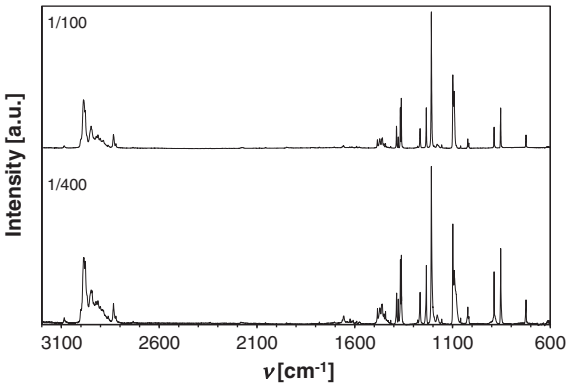

Fig. 5. MIR spectrum of TBME in Argon matrix (12 K, 1/100 and 1/400) in the 3200–600 cm^{-1} range.

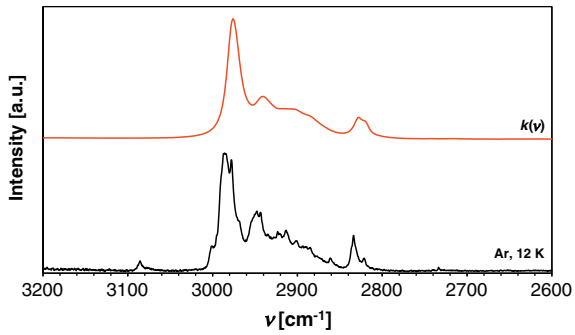

Fig. 6. Details of MIR spectra of TBME: in Ar matrix (12 K, 1/100) and $k(\nu)$ in the 3200–2600 cm^{-1} range.

of TBME is a step needed for the following studies of dielectric properties of examined liquid.

The theoretical IR spectrum of TBME was obtained from anharmonic vibrational frequencies calculated in Gaussian 09 [17]. The TBME molecule scheme is presented in Fig. 9. The internal coordinates constructed in accordance with Pulay et al. [18] are presented in Table 1. We have chosen the Cauchy–Gauss product function [19] as the band model, with a constant Cauchy/Gauss ratio and a constant half-width of the bands (14 cm^{-1}). A modeled vibrational spectrum compared with experimental $k(\nu)$ is presented in Figs. 10 and 11. Amplified segments of spectra are presented for a better view of details.

The accuracy of spectra simulation is noticeably higher in the lower MIR region, similarly as in our previous studies [20,21]. The observed differences in the C–H stretching region cannot be explained by any meaningful aggregation of the liquid. Moreover, there are no proton donor groups in the studied molecule, therefore no association due to hydrogen-bonding is expected. No evidence was also found in literature for other types of structure-making forces in liquid ethers, e.g. due to dipole–dipole interactions, since the dipole moment of TBME amounts only to 1.4 D [22]. Both the spectrum recorded in solution and at low temperatures share the broadened bands observed in the C–H stretching region of $k(\nu)$ spectrum of neat liquid TBME.

4.5. Identification of bands in MIR region

The identification of bands observed in liquid phase spectra was based on a potential energy distribution (PED) [23] analysis. The obtained PED for TBME is presented in Table 2 and the resulting band identifications are presented in Table 3.

As stated previously, the quality of prediction of the experimental spectrum is lower in the C–H stretching region — both in terms of band positions and relative intensities, resulting in an overall different spectrum shape. Nevertheless major bands can still be identified. The CH_3 stretching antisymmetric and antisymmetric′, as well stretching

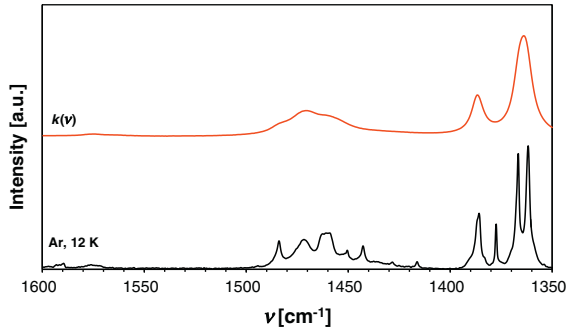

Fig. 7. Details of MIR spectra of TBME: in Ar matrix (12 K, 1/100) and $k(\nu)$ in the 1600–1350 cm^{-1} range.

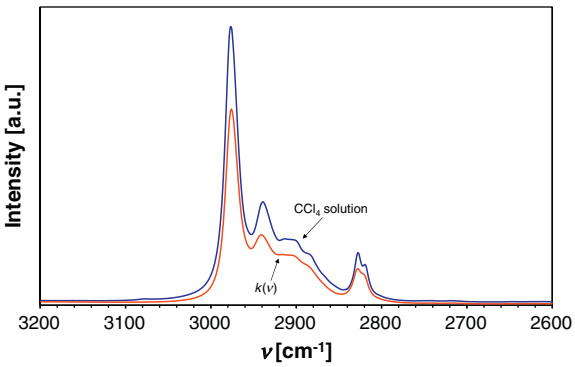

Fig. 8. Comparison of the absorption spectrum of 0.3 M TBME solution in carbon tetrachloride (140 μm cell) with $k(\nu)$ spectrum of TBME in the 3200–2600 cm^{-1} range.

symmetric modes for those groups have been identified (Table 3). There can also be noticed a distinguishable dual band peaking at 2827.8 cm^{-1} and ~2819 cm^{-1}. The obtained computational results suggest that at least one of those bands, most probably the 2827.8 cm^{-1} one, originates from the symmetric stretching vibration of a methyl group connected directly to an oxygen atom. In this mode there's also a minor addition of symmetric stretching modes of other CH_3 groups present in the TBME molecule. It is worth mentioning that unlike for some other aliphatic ethers examined before [24,25], the TBME spectrum in this region does not exhibit any bands at wavenumbers lower than 2800 cm^{-1}.

The broadened structure observed in the $k(\nu)$ spectrum between 2940 cm^{-1} and 2870 cm^{-1} remains also in the low concentration solution spectrum in CCl_4 and in the low-temperature matrix spectra as well. Due to significantly lower half-widths of bands in the low temperature spectra it can be however estimated that at least 5 distinctive peaks may contribute into it. Those peaks are located at 2923, 2913, 2902, 2886 and 2862 cm^{-1} (Fig. 6). Basing on the obtained results of the computational studies the origin of those bands cannot be explained. However in this region the occurrence of Fermi resonance bands formed as a result of an interaction of the first overtone of CH_3 deformation vibrations and fundamental CH_3 stretching vibrations can be expected [26].

The lower MIR region can be explained thoroughly thanks to the high accuracy of the model spectrum. The discussed region is dominated by

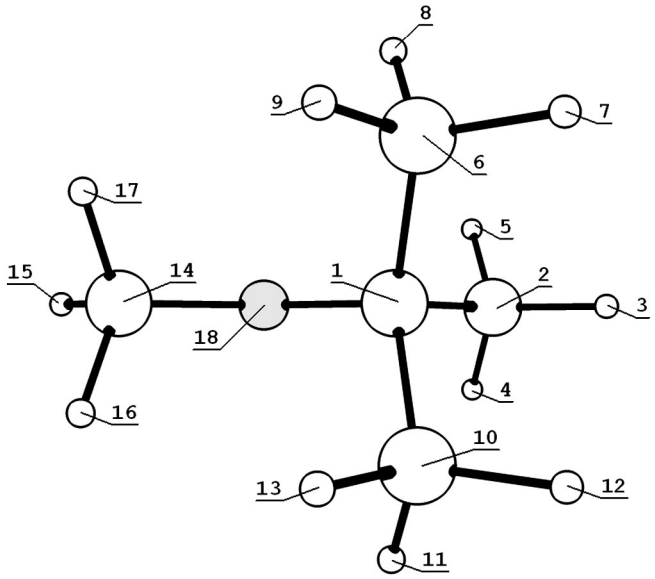

Fig. 9. Assumed atom numbering in TBME molecule.

Table 1
Internal coordinates table for TBME.

Coord.no.	Description	Coord.no.	Description
1	C1 – C2 stretch.	25	$C(10)H_3$ asym.def.′
2	C1 – C6 stretch.	26	$C(10)H_3$ rock.
3	C1 – C10 stretch.	27	$C(10)H_3$ rock.′
4	C1 – O18 stretch.	28	$C(6)H_3$ sym. def.
5	C2 – H3 stretch.	29	$C(6)H_3$ asym.def.
6	C2 – H4 stretch.	30	$C(6)H_3$ asym.def.′
7	C2 – H5 stretch.	31	$C(6)H_3$ rock.
8	C6 – H7 stretch.	32	$C(6)H_3$ rock.′
9	C6 – H8 stretch.	33	$C(2)H_3$ sym. def.
10	C6 – H9 stretch.	34	$C(2)H_3$ asym.def.
11	C10 – H11 stretch.	35	$C(2)H_3$ asym.def.′
12	C10 – H12 stretch.	36	$C(2)H_3$ rock.
13	C10 – H13 stretch.	37	$C(2)H_3$ rock.′
14	C14 – H15 stretch.	38	H15 – C14 – O18 – C1 tors.
15	C14 – H16 stretch.	39	C2 – C1 – O18 – C14 tors.
16	C14 – H17 stretch.	40	C2 – C1 – C10 – H11 tors.
17	C14 – O18 stretch.	41	C2 – C1 – C6 – H7 tors.
18	$C(14)H_3$ sym. def.	42	C6 – C1 – C2 – H3 tors.
19	$C(14)H_3$ asym.def.	43	C1 – O18 – C14 bend.
20	$C(14)H_3$ asym.def.′	44	O18 – C1 – C2 bend.
21	$C(14)H_3$ rock.	45	O18 – C1 – C6 bend.
22	$C(14)H_3$ rock.′	46	C2 – C1 – C6 bend.
23	$C(10)H_3$ sym. def.	47	C2 – C1 – C10 bend.
24	$C(10)H_3$ asym.def.	48	C6 – C1 – C10 bend.

CH_3 deformation bands, both symmetric and antisymmetric (in the 1500–1300 cm^{-1} range), and C – O stretching and C – C stretching modes with an addition of CH_3 rocking and OCC bending modes (in the 1300–1000 cm^{-1} range). A very intense band of C – O stretching mode can be seen at 1086 cm^{-1}, a distinctly lower wavenumber when compared with the same band in the spectra of the aliphatic ethers studied earlier [24,25]. Finally, in the relatively uncomplicated 1000–560 cm^{-1} range we observe CH_3 rocking and C – O stretching bands.

The 1500–1350 cm^{-1} region of the $k(\nu)$ spectrum can be elucidated even further by examining the low-temperature spectra (Fig. 7 and Table 4). The broad $k(\nu)$ band at 1470.5 cm^{-1} becomes in the low-temperature spectrum, four clearly separated bands at 1484, 1472, 1461 and 1450 cm^{-1}. All these bands originate from methyl asymmetric and asymmetric′ deformation modes. Further, bands observed at 1386.7 cm^{-1} and at 1363.9 cm^{-1} in the $k(\nu)$ spectrum can be distinguished in the low-temperature spectrum as four bands (at 1386, 1377, 1367 and 1362 cm^{-1}). These bands were identified as methyl symmetric deformation bands (Table 4).

5. Summary

Basing on IR studies including thin film MIR transmission recordings, the spectrum of the complex refractive index for liquid *tert*-butylmethylether (TBME) was determined in a broad spectral

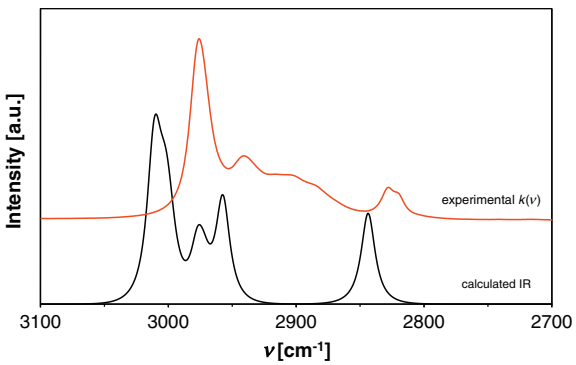

Fig. 10. Experimental $k(\nu)$ and calculated IR spectra of TBME in the upper MIR range (3100–2700 cm^{-1}).

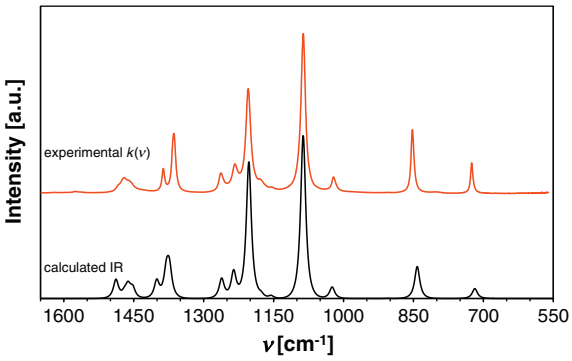

Fig. 11. Experimental $k(\nu)$ and calculated IR spectra of TBME in the lower MIR range (1650–550 cm^{-1}).

range (11,700–560 cm^{-1}). The experiment was supported by low-temperature matrix isolation studies, which allowed for a more thorough insight into factors determining the details of IR spectrum of TBME. An anharmonic vibrational analysis was performed on a B2PLYP/N07D

Table 3
Band identification in MIR and Raman spectra of liquid TBME.

	ν_{exp} [cm^{-1}]		ν_{calc} [cm^{-1}]	Vibrational modes contribution
	IR	Raman		
1	2976.0	2977.6	3011	CH_3 asym. stretch.
2	2940.0	–	2957	CH_3 asym.′ stretch.
3	~2918	~2914	–	CH_3 symm. stretch.
4	~2904	–	–	–
5	~2884	~2880	–	–
6	2827.8	2828.1	2843	(α–)CH_3 symm. stretch.
7	1470.5	~1466	1488	CH_3 asym.′ def.
8	1386.7	–	1400	CH_3 symm. def.
9	1363.9	1362.3	1373	CH_3 symm. def.
10	1263.1	1263.6	1261	C–C stretch., O–C–C(H_3) bend.
11	1204.5	1203.8	1203	C–O stretch., CH_3 rock.
12	1181.0	1177.5	1176	CH_3 rock.
13	1086.3	1085.9	1086	C–O stretch.
14	1021.5	1021.9	1023	CH_3 rock.
15	852.4	852.0	842	C–O stretch.
16	725.2	725.5	718	C–O stretch.

Table 2
PED table for TBME (B2PLYP/N07D).

	ν(harm) [cm^{-1}]	Mode	(%)	Mode	(%)	Mode	(%)	Mode	(%)	Mode	(%)	Mode	(%)	Mode	(%)	Mode	(%)	Mode	(%)
1.	50.25	39	(59.)	38	(23.)	45	(6.)												
2.	178.48	38	(28.)	−40	(26.)	−41	(26.)	−42	(15.)										
3.	231.97	42	(69.)	38	(21.)														
4.	257.52	41	(34.)	−40	(34.)	−43	(15.)	44	(10.)										
5.	282.00	41	(30.)	−42	(25.)	40	(21.)	38	(13.)										
6.	288.75	44	(41.)	−43	(20.)	40	(13.)	48	(9.)										
7.	343.55	45	(34.)	−46	(26.)	47	(26.)												
8.	367.93	48	(34.)	43	(23.)	−46	(15.)	−47	(14.)										
9.	415.91	48	(40.)	47	(21.)	46	(20.)	36	(6.)										
10.	462.31	45	(57.)	−47	(10.)	46	(9.)	−37	(5.)										
11.	510.15	43	(33.)	44	(27.)	46	(8.)	47	(8.)	27	(6.)	1	(5.)						
12.	733.30	4	(28.)	3	(23.)	2	(23.)	1	(13.)										
13.	868.24	4	(40.)	−1	(11.)	−2	(8.)	17	(8.)	−3	(8.)	36	(6.)						
14.	924.63	2	(21.)	−3	(21.)	31	(17.)	26	(16.)	37	(10.)	−27	(5.)	−32	(5.)				
15.	935.83	1	(28.)	36	(21.)	−27	(15.)	−32	(11.)	−31	(7.)	−3	(6.)	−2	(6.)				
16.	966.06	37	(33.)	32	(31.)	−26	(20.)	−27	(12.)										
17.	1046.96	27	(29.)	−31	(26.)	37	(19.)	−45	(6.)	−3	(5.)								
18.	1053.45	36	(32.)	26	(20.)	32	(13.)	−31	(9.)	17	(6.)								
19.	1122.50	17	(74.)	−4	(10.)														
20.	1184.88	22	(94.)																
21.	1214.49	21	(62.)	26	(5.)	48	(5.)												
22.	1241.38	4	(23.)	−31	(10.)	−36	(10.)	−21	(10.)	−27	(8.)	46	(8.)	47	(8.)	48	(6.)	48	(6.)
23.	1273.08	37	(19.)	−2	(18.)	3	(18.)	45	(10.)	26	(6.)	−47	(5.)	46	(5.)				
24.	1304.03	1	(23.)	−44	(10.)	32	(9.)	−43	(7.)	−21	(6.)	27	(6.)						
25.	1409.22	28	(47.)	−23	(40.)	2	(6.)												
26.	1413.05	33	(47.)	−23	(21.)	−28	(16.)	1	(8.)										
27.	1435.46	33	(40.)	23	(26.)	28	(25.)												
28.	1484.95	18	(76.)	−30	(7.)														
29.	1485.81	34	(29.)	−24	(19.)	29	(16.)	−35	(11.)	−25	(7.)	−19	(5.)						
30.	1500.03	30	(22.)	29	(21.)	25	(20.)	−24	(20.)	19	(5.)								
31.	1502.41	35	(45.)	34	(16.)	25	(8.)	−30	(7.)	−24	(6.)	−29	(5.)						
32.	1507.67	19	(28.)	34	(27.)	−35	(11.)	−20	(9.)										
33.	1514.24	24	(28.)	29	(26.)	−18	(10.)	20	(9.)										
34.	1522.52	19	(31.)	−30	(18.)	−25	(16.)	−20	(13.)	−34	(5.)								
35.	1528.31	20	(51.)	19	(19.)	−21	(8.)	−24	(6.)										
36.	1535.70	30	(26.)	−25	(26.)	35	(15.)	18	(6.)	34	(5.)								
37.	3033.86	16	(45.)	15	(45.)	14	(9.)												
38.	3065.61	12	(17.)	−8	(17.)	11	(16.)	13	(16.)	−10	(16.)	−9	(16.)						
39.	3068.04	5	(21.)	6	(16.)	7	(16.)	−8	(9.)	−12	(8.)	−9	(8.)	−11	(8.)	−10	(7.)	−13	(7.)
40.	3074.77	5	(17.)	7	(15.)	6	(15.)	11	(9.)	9	(9.)	8	(9.)	12	(8.)	10	(8.)	13	(8.)
41.	3093.74	15	(48.)	−16	(48.)														
42.	3142.23	8	(30.)	−12	(25.)	−10	(22.)	13	(18.)										
43.	3145.76	12	(27.)	8	(22.)	−5	(13.)	−13	(11.)	−10	(9.)								
44.	3150.82	11	(40.)	−13	(24.)	−9	(15.)	−6	(7.)										
45.	3151.24	10	(29.)	−9	(28.)	−5	(14.)	13	(11.)	7	(7.)								
46.	3155.97	5	(34.)	−9	(13.)	−11	(12.)	−6	(11.)	−7	(9.)	8	(8.)	12	(8.)				
47.	3157.33	7	(45.)	−6	(45.)														
48.	3159.07	14	(82.)																

Table 4
Detailed band identification in the range 1500 – 1350 cm^{-1} of infrared spectra of TBME.

	ν_{exp} [cm^{-1}]		ν_{teor} [cm^{-1}]	Assignments
	$k(\nu)$	Ar matrix (12 K)		
1	1470.5	1483.9	1488	CH_3 asym. def.′
2		1472.3	1469	CH_3 asym. def.
3		1461.3	1462	CH_3 asym. def.
4		1450.4	1449	CH_3 asym. def.′
5	1386.7	1385.8	1400	CH_3 symm. def.
6		1377.4	–	–
7	1363.9	1366.5	1380	CH_3 symm. def.
8		1361.7	1374	CH_3 symm. def.

level of theory. The experimental spectrum of the absorption coefficient was accurately simulated, and a successful identification of numerous MIR bands of the studied liquid was carried out.

Acknowledgement

We wish to thank Prof. Z. Mielke for the helpful discussions.

Calculations have been partially carried out in the Wroclaw Centre for Networking and Supercomputing (http://www.wcss.wroc.pl), grant No. 20207.

References

[1] E.D. Radchenko, R. Chikosh, B.A. Énglin, I. Palai, Yu A. Robert, Ya Laki, G.I. Levinson, A. Tot, L.V. Malyavinskii, Yu.N. Nilov, F.V. Turovskii, Chem. Tech. Fuels Oil 12 (1976) 336.
[2] L.M. Noreiko, S.A. Feigin, E.D. Radchenko, A.V. Agafonov, G.P. Klishina, Chem. Tech. Fuels Oil 15 (1979) 338.
[3] M.A. Krähenbühl, J. Gmehling, J. Chem. Eng. Data 39 (1994) 759.
[4] T. Zhang, J. Wang, T. Yuan, X. Hong, L. Zhang, F. Qi, J. Phys. Chem. A 112 (2008) 10487.
[5] P.J. Squillace, J.F. Pankow, N.E. Korte, J.S. Zogorski, Environ. Toxicol. Chem. 16 (1997) 1836.
[6] A. François, H. Mathis, D. Godefroy, P. Piveteau, F. Fayolle, F. Monot, Appl. Environ. Microbiol. 68 (2002) 2754.
[7] M.M. Häggblom, L.K.G. Youngster, P. Somsamak, H.H. Richnow, Adv. Appl. Microbiol. 62 (2007) 1.
[8] G. De Palma, D. Poli, P. Manini, R. Andreoli, P. Mozzoni, P. Apostoli, A. Mutti, Biomarkers 17 (2012) 343.
[9] M. Winterberg, E. Schulte-Korne, U. Peters, F. Nierlich, Methyl Tert-Butyl Ether in Ullmann's Encyclopedia of Industrial Chemistry, Wiley-VCH, Weinheim, 2010.
[10] 2006. SCOEL/SUM/110.
[11] J.P. Hawranek, P. Neelakantan, R.P. Young, R.N. Jones, Spectrochim. Acta 32A (1976) 75.
[12] W. Wrzeszcz, A.S. Muszyński, J.P. Hawranek, Comput. Chem. 22 (1998) 101.
[13] J.P. Hawranek, A.S. Muszyński, Comput. Chem. 22 (1998) 95.
[14] R.G. Snyder, G. Zerbi, Spectrochim. Acta A 23 (1967) 391.
[15] B.I. Łydżba-Kopczyńska, K.B. Beć, J. Tomczak, J.P. Hawranek, J. Mol. Liq. 172 (2012) 34.
[16] M. Biczysko, P. Panek, G. Scalmani, J. Bloino, V. Barone, J. Chem. Theory Comput. 6 (2010) 2115.
[17] M.J. Frisch, G.W. Trucks, H.B. Schlegel, G.E. Scuseria, M.A. Robb, J.R. Cheeseman, G. Scalmani, V. Barone, B. Mennucci, G.A. Petersson, H. Nakatsuji, M. Caricato, X. Li, H. P. Hratchian, A.F. Izmaylov, J. Bloino, G. Zheng, J.L. Sonnenberg, M. Hada, M. Ehara, K. Toyota, R. Fukuda, J. Hasegawa, M. Ishida, T. Nakajima, Y. Honda, O. Kitao, H. Nakai, T. Vreven, J.A. Montgomery Jr., J.E. Peralta, F. Ogliaro, M. Bearpark, J.J. Heyd, E. Brothers, K.N. Kudin, V.N. Staroverov, R. Kobayashi, J. Normand, K. Raghavachari, A. Rendell, J.C. Burant, S.S. Iyengar, J. Tomasi, M. Cossi, N. Rega, J.M. Millam, M. Klene, J.E. Knox, J.B. Cross, V. Bakken, C. Adamo, J. Jaramillo, R. Gomperts, R.E. Stratmann, O. Yazyev, A.J. Austin, R. Cammi, C. Pomelli, J.W. Ochterski, R.L. Martin, K. Morokuma, V.G. Zakrzewski, G.A. Voth, P. Salvador, J.J. Dannenberg, S. Dapprich, A.D. Daniels, O. Farkas, J.B. Foresman, J.V. Ortiz, J. Cioslowski, D.J. Fox, Gaussian 09, Revision A.02, Gaussian, Inc., Wallingford CT, 2009.
[18] P. Pulay, G. Fogarasi, F. Pang, J.E. Boggs, J. Am. Chem. Soc. 101 (1979) 2550.
[19] J.P. Hawranek, Acta Phys. Polon. A40 (1971) 811.
[20] A.S. Muszyński, K.B. Beć, W. Wrzeszcz, N. Michniewicz, A. Mojak, J.P. Hawranek, J. Mol. Struct. 975 (2010) 205.
[21] K.B. Beć, J.P. Hawranek, J. Mol. Struct. 1026 (2012) 51.
[22] J.A. Riddick, W.B. Bunger, T.K. Sakano, Fourth edition, Organic Solvents, vol. II, John Wiley and Sons, New York, 1986.
[23] J.M.L. Martin, C. Van Alsenoy, GAR2PED (University of Antwerp), 1995.
[24] K.B. Beć, J.P. Hawranek, Vib. Spectrosc. 64 (2013) 164.
[25] K.B. Beć, J.P. Hawranek, J. Spectrosc. 705218 (2013) 1.
[26] D.C. McKean, Spectrochim. Acta A 29 (1973) 1559